Surface Science 296 (1993) 299–309
North-Holland

surface science

STM investigations of solid surfaces in water and air

J.P. Song [a,b,c], K.A. Mørch [a], K. Carneiro [b] and A.R. Thölén [a]

[a] *Physics Department, Building 307, Technical University of Denmark, DK-2800 Lyngby, Denmark*
[b] *Danish Institute of Fundamental Metrology, Building 307, Lundtoftevej 100, DK-2800 Lyngby, Denmark*
[c] *Department of Electronic Engineering, Xi'an Jiaotong University, Xi'an, People's Republic of China*

Received 25 February 1993; accepted for publication 16 July 1993

Scanning tunneling microscopy (STM) investigations on nonplanar surface elements of different specimen materials are carried out in atmospheric air and when they are covered with distilled water in order to determine effects of water on the recorded surface topography and the tunneling barrier. When water is supplied to a dry specimen surface small scale topographic irregularities (up to about 0.2 μm) are found to be smoothed and characteristic changes are observed in the tunneling barrier signals of the investigated materials. The observed topographic changes in water are expected to be caused by nano-voids formed by detachment of the liquid from concave surface elements. During scanning the STM tips were found to be worn, particularly when scanning in air on some of the non-noble metals, much less in water. As wear affects the resolution of the STM it may be an advantage to scan in water instead of in air if locally the specimen has a poor conductivity, but the possibility that the recorded interface topography is affected by the water must be taken into consideration. Further, the level of the tunneling barrier signals of different materials and their change at exposure to water instead of air can be used for detecting nucleation of surface coatings.

1. Introduction

STM investigations of solid surfaces in water were first described by Sonnenfeld and Hansma [1] who found no evidence of influence of the aqueous environment on the recorded surface topography of their specimens. The technique has also been developed for underwater STM of organic and biological molecules [2,3] and for studies of in situ electrode surfaces [4,5]. A direct STM comparison of non-planar solid surfaces exposed to air and water at identical locations has apparently not been made, probably because effects of the liquid were not expected. However, it is known that the tensile strength of water is decisively reduced by the presence of solid surfaces, even small particles [6], which are sites of weak points. An orderly structure of the water molecules in the vicinity of a solid surface was already discussed by Drost-Hansen [7] and recently a model of cavitation inception (the transient growth of cavitation nuclei into vapour cavities) in water based on an ice-Ih structure near solid surfaces has been proposed [8,9]. The STM technique seems the only one which opens up the possibility of investigating on a nanometer scale the interface between solids and water, and thus of identifying possible cavitation nuclei.

By measurements in air, Everson and Tamor [10] found that changes of the tunneling barrier signal between areas of a substrate covered with boron-doped diamond crystals and areas which were not covered were an effective means of identifying microcrystals. In refs. [11,12], tunneling barriers in the range of 0.1 eV up to values approaching the work functions are reported for W–Au and W–Pt tunneling. The highest values were obtained by effectively cleaning the tip and specimen, and in ref. [11] a value of 3.2 eV was achieved when the pressure was reduced to about 10^{-6} Torr. Thus, contamination, oxidation and physisorption of gas molecules seem decisive for the tunneling barrier. In the present paper, tunneling barrier signals and surface topography are

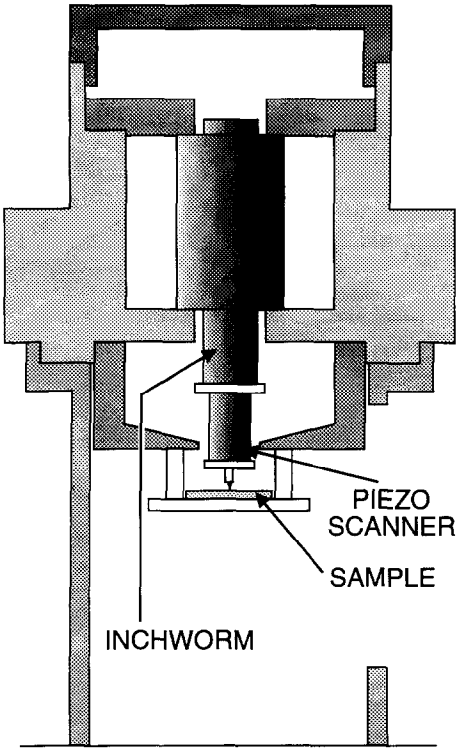

Fig. 1. STM setup for investigation of surfaces in air and water. A tiny drop of water can be injected onto or sucked away from specimen surface.

investigated in air and in water by numerous scannings with W- and Pt-tips on several specimens made from W, Au and TiN.

2. Experiments

For the present investigation, a STM with an axially symmetric structure, as shown in fig. 1, was designed and built in our laboratory [13]. The construction minimizes the thermal drift of the STM images in the x- and y-directions. An inchworm motor (Burleigh) is used for coarse adjustment of the tip–sample distance and a piezoelectic tube-scanner (EBL Company) is used for scanning and for fine adjustments of the tip movements in the x-, y- and z-directions.

The STM was operated in constant current mode, the z-voltage applied to the tube scanner thus giving the surface topography. Tunneling barrier investigations were made by superposing a 30 mV peak-to-peak oscillation at 1.0 kHz on the instantaneous servo-controlled z-voltage to generate a small oscillation of the STM tip. With a z-sensitivity of the piezo-scanner of 4.7 nm/V found by calibration in a Michelson interferometer, we estimate the peak-to-peak oscillation to be $\delta s \approx 0.14$ nm. The resulting 1 kHz fluctuation of the tunneling current, δI_t, is detected in a lock-in amplifier and a signal $\mathrm{d}(\ln I_t)/\mathrm{d}s$ proportional to $\phi^{1/2}$ is calculated, where ϕ is the value of the tunneling barrier, and s is the tip–sample distance. The topographic signals and the tunneling barrier signals are recorded simultaneously in images of each 128×128 pixels. This allows accurate comparison of the tunneling barrier signal with the surface topography signal. The recording time for each picture was about 20 min. or about 30 ms per pixel. With a time constant of the lock-in amplifier also of 30 ms the resolution of the barrier signal is about 1 pixel, and the signal is averaged from about 30 tip oscillations. Thus the tunneling barrier signal represents the local average barrier, and in each point its uncertainty can be considered to be less than 10%.

More detailed investigations of tunneling barrier signals with a sample-and-hold technique, in which the feed-back loop is broken during one or two pairs of tip motion in forward and backward z-direction, show that in air an almost linear $\ln I_t$ versus s relationship is obtained, see fig. 2A, in agreement with earlier findings in the literature [11,12]. In water the relationship is more complicated, often the $\ln I_t$ versus s curve is made up from more than one linear relationship, which varies from one measurement to the next, and it may depend on the direction of the tip z-displacement, examples are shown in figs. 2B and 2C [14,15]. Thus, in air a well-defined tunneling barrier exists. In water, the piece by piece linear relationships each can be taken to define a tunneling barrier, though it may shift during measurement of the barrier signal. However, with the lock-in technique, by which a smoothed current signal is recorded over several tip z-oscillations, only an apparent tunneling barrier signal is determined in water. The bias voltage was in each case

chosen so that in water the Faradaic current was as close as possible to zero, and therefore its possible influence on the tunneling barrier signal could not be investigated with the tips used. For given tip and specimen the tunneling current and the bias voltage were, for the purpose of comparison, kept at the same values at measurements in air as in water.

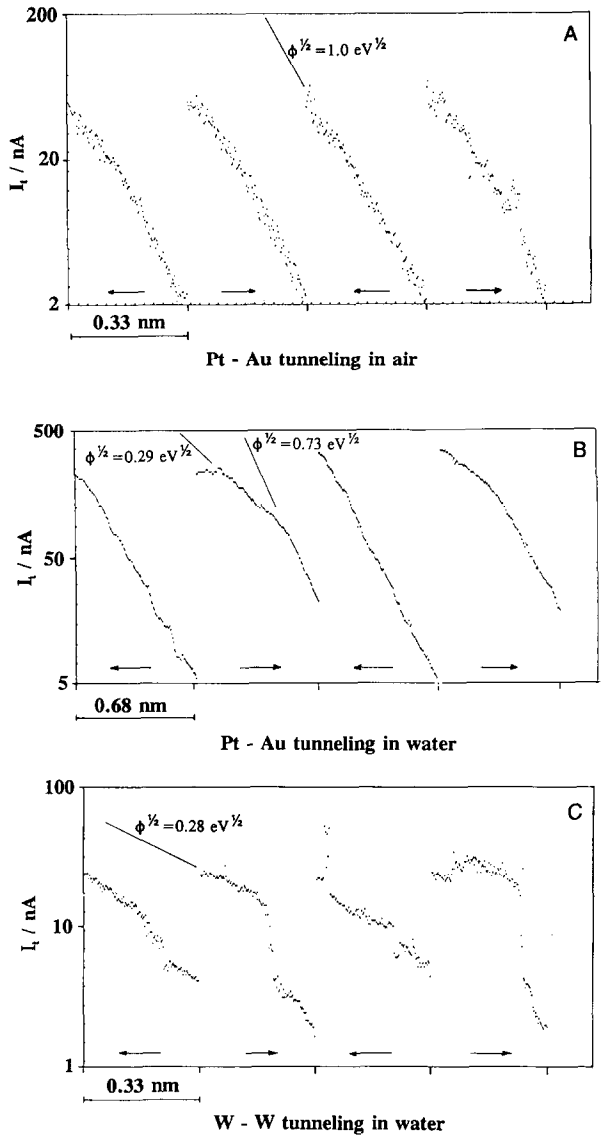

Fig. 2. Tunneling current I_t vs. tip–specimen distance s: (A) in air at Pt–Au tunneling; (B) in water at Pt–Au tunneling; (C) in water at W–W tunneling (newly etched specimen). The arrows at each curve show the direction of tip motion. The tunneling current feedback loop is activated between each pair of forward and backward tip motion, carried out in 700 ms. $\phi^{1/2}$ values corresponding to different line inclinations are shown in the figures.

The specimen was horizontally placed below the STM tip, and a tiny drop of distilled water was injected onto (or removed from) the specimen surface with a pipette at the position of the tip. Thus the specimen area to be investigated and part of the tip cone were embraced by the drop, but the drop was not in contact with any other material component. Sharp tungsten STM tips with tip radii of about 15 nm, made by a second-etching method [16], and simply cut platinum tips were used. Specimens of tungsten and gold as well as specimens with TiN crystals grown on a tungsten substrate were investigated at exposure to air and to water. These investigations are described and illustrated by representative STM images selected from a large number of scannings.

When water is supplied to (or removed from) a specimen surface the STM tip is inevitably moved from its original position. However, careful operation minimizes the displacement in the x and y directions to about 0.1 μm, and at surface locations which show characteristic features the tip can generally be relocated by adjusting the (x, y)-offset voltages on the tube-scanner so that very precisely the same surface element is scanned when covered and when not covered with water.

For operation of the STM in water the bias voltage had to be carefully adjusted to balance the electrochemical potentials of the tip and specimen materials because the tips were not electrically insulated. Hereby it was possible to ensure that the Faradaic current was negligible (< 0.5 nA). This balancing was carried out with the tip out of tunneling distance before each scanning, and it was controlled immediately after. The tunneling current was chosen to be $I_t = 4.0$ nA.

By measurements with a tungsten tip on a tungsten specimen in water the bias voltage of the tip was a few mV only when the Faradaic current was cancelled, because the two material components were almost identical. Figs. 3A and 3B show an example of a pair of "four-dimen-

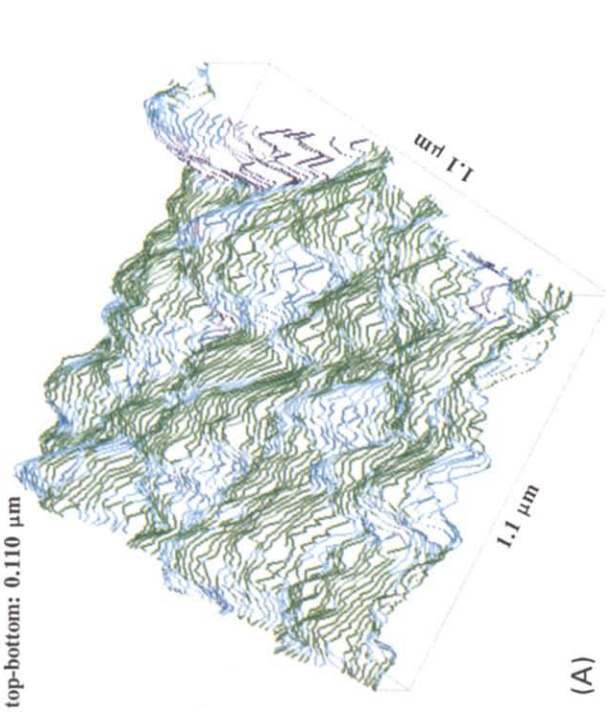
top-bottom: 0.110 μm
1.1 μm
1.1 μm
(A)

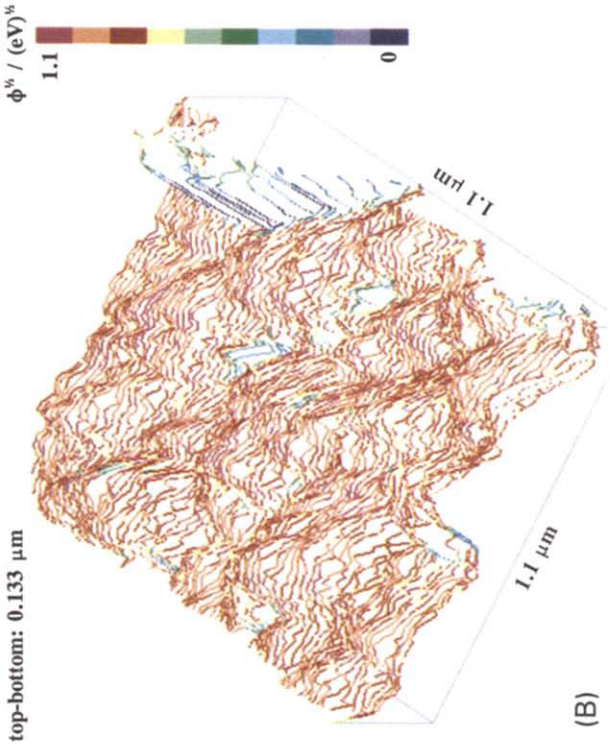
$\phi^{1/2}$ / (eV)$^{1/2}$
1.1
0
top-bottom: 0.133 μm
1.1 μm
1.1 μm
(B)

Fig. 4.

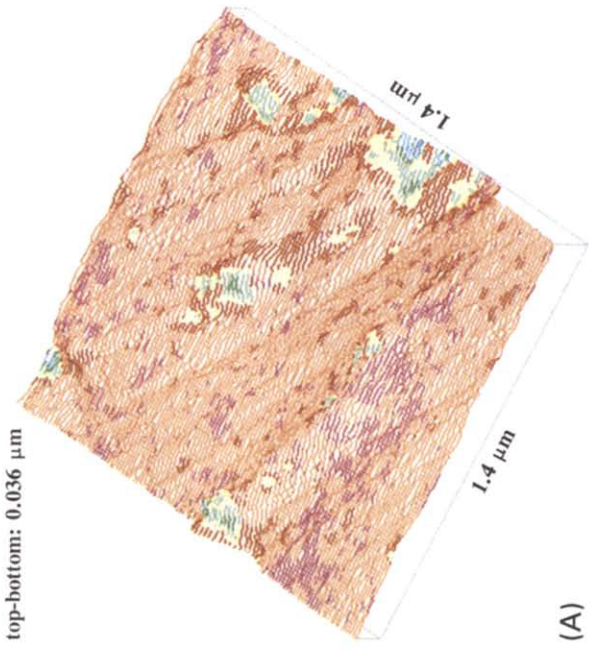
top-bottom: 0.036 μm
1.4 μm
1.4 μm
(A)

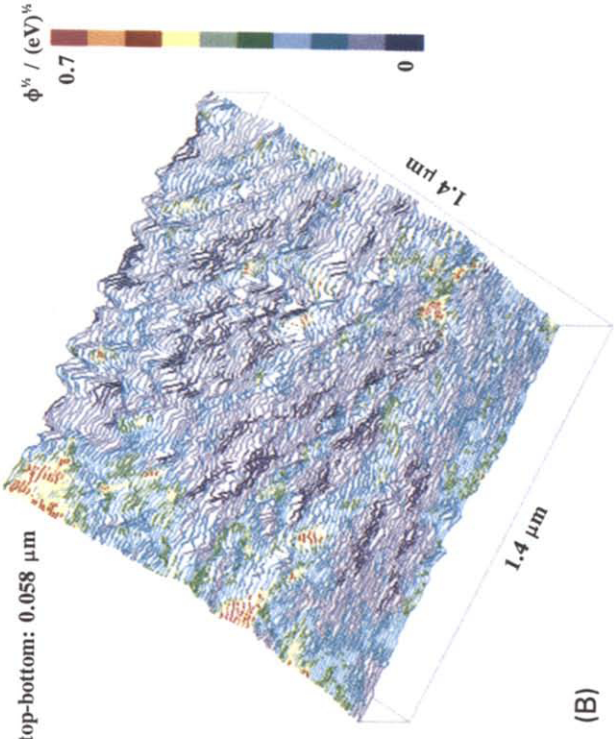
$\phi^{1/2}$ / (eV)$^{1/2}$
0.7
0
top-bottom: 0.058 μm
1.4 μm
1.4 μm
(B)

Fig. 3.

sional" STM images (which are tilted 30°) of a tungsten specimen, obtained with a sharp tungsten STM tip. The specimen was prepared by grinding and polishing. As W is highly reactive all W-surfaces can be considered covered by at least thin layers of oxides. The scan lines in these pictures present the three-dimensional surface topography, as usual in STM, and as a fourth dimension the colour indicates the level of the local tunneling barrier signal, $\phi^{1/2}$, obtained simultaneously by the lock-in amplifier technique described above. The tungsten surface exposed to water, shown in fig. 3A, was recorded first in order to have the sharpest possible tip during this scanning and thus the highest possible resolution of the STM. Then the surface was drained so that the tungsten surface was exposed to air, and the image shown in fig. 3B was obtained at almost the same location. After draining of the surface some water molecules may still be adsorbed to the W-surface, but the tunneling barrier signals of the W-surfaces in air are found to be the same before being exposed to water as after being drained. Further, on the drained specimens no Faradaic current could be measured at the change of the bias voltage, which supports that the tunneling gap was an air gap. The scanned area is about 1.4×1.4 μm^2. The top–bottom distance indicates the z-level difference between the highest peak and the deepest pit (or valley) (the latter determines the bottom plane of the depicted volume). The level of the local tunneling barrier signal, $\phi^{1/2}$, is given by the colour scale bar in the right of the picture (the bar is linear in $\phi^{1/2}$, increasing from 0 $(eV)^{1/2}$ at dark violet to 0.7 $(eV)^{1/2}$ at magenta). With the tungsten sample exposed to water (fig. 3A) the range of $\phi^{1/2}$ was ~ 0.5–0.7 $(eV)^{1/2}$ at most of the interface, while in air (fig. 3B) it is predominantly less than 0.3 $(eV)^{1/2}$. In water some small regions with a lower tunneling barrier signal and in air some small regions with a higher tunneling barrier signal than those mentioned above are present too. The anomalous regions may be caused by contamination, as the specimen was cleaned only with distilled water before being investigated, and on the drained surface maybe by residual water molecules. However, the general feature is that the tunneling barrier signals are distinctly different in the two cases, and that they are higher in water than in air by W–W tunneling. The numerical results obtained are reproducible by successive scans as well as by repeated investigation after half a year when due to ageing the thickness of the tungsten oxide layer covering the specimen surface has probably increased. In water the surface topography of the investigated specimen appears very smooth, essentially only a weak ripple structure is discernible. In air the ripple structure is much more prominent, with deeper valleys and small-scale irregularities, in particular in the upper half of fig. 3B. The scanning starts in the upper right corner of each picture. Probably increasing tip wear during scanning on the drained surface reduces the resolution of the STM, so that the topographic irregularities are not recorded towards the end of the scanning shown in fig. 3B.

In figs. 4A and 4B an area of 1.1×1.1 μm^2 of a specimen made from gold vacuum deposited on a flat substrate is shown as recorded with a platinum tip at exposure to water and to air, respectively. Fig. 4B is recorded before fig. 4A. The bias voltage of the tip was about +100 mV. The tunneling barrier signal at Pt–Au tunneling in water is less than 0.5 $(eV)^{1/2}$, while in air it is

Fig. 3. "Four-dimensional" STM images of an area of 1.4×1.4 μm^2 of a tungsten specimen recorded with a tungsten STM tip. First (A) was obtained by scanning in water. Then the specimen surface was drained and at almost the same location (B) was obtained in air. The level of the local tunneling barrier signal is indicated by the colour scale bar (dark violet $\phi^{1/2} \approx 0$ $(eV)^{1/2}$, magenta $\phi^{1/2} \approx 0.7$ $(eV)^{1/2}$). For W–W tunneling the barrier signal increases when water is supplied to the interface.

Fig. 4. "Four-dimensional" STM images of an area of 1.1×1.1 μm^2 of a gold specimen recorded with a cut platinum STM tip. (A) was obtained in water after (B) had been recorded in air. For Au–Pt tunneling the barrier signal decreases when water is supplied to the interface. The level of the local tunneling barrier signal is indicated by the colour scale bar (dark violet $\phi^{1/2} \approx 0$ $(eV)^{1/2}$, magenta $\phi^{1/2} \approx 1.1$ $(eV)^{1/2}$).

predominantly 0.8–1.1 $(eV)^{1/2}$. This result has proved reproducible in several experiments. The simply cut platinum tip was very jagged and blunt. Therefore, the point of tunneling may have shifted in dependence of the specimen topography, and it is difficult to conclude about the topography in detail. When scanning on non-planar surfaces over a large range a reliable nanometer scale resolution was achieved only with the sharp tungsten tips.

A tungsten specimen partially coated with an object material and scanned with a tungsten tip

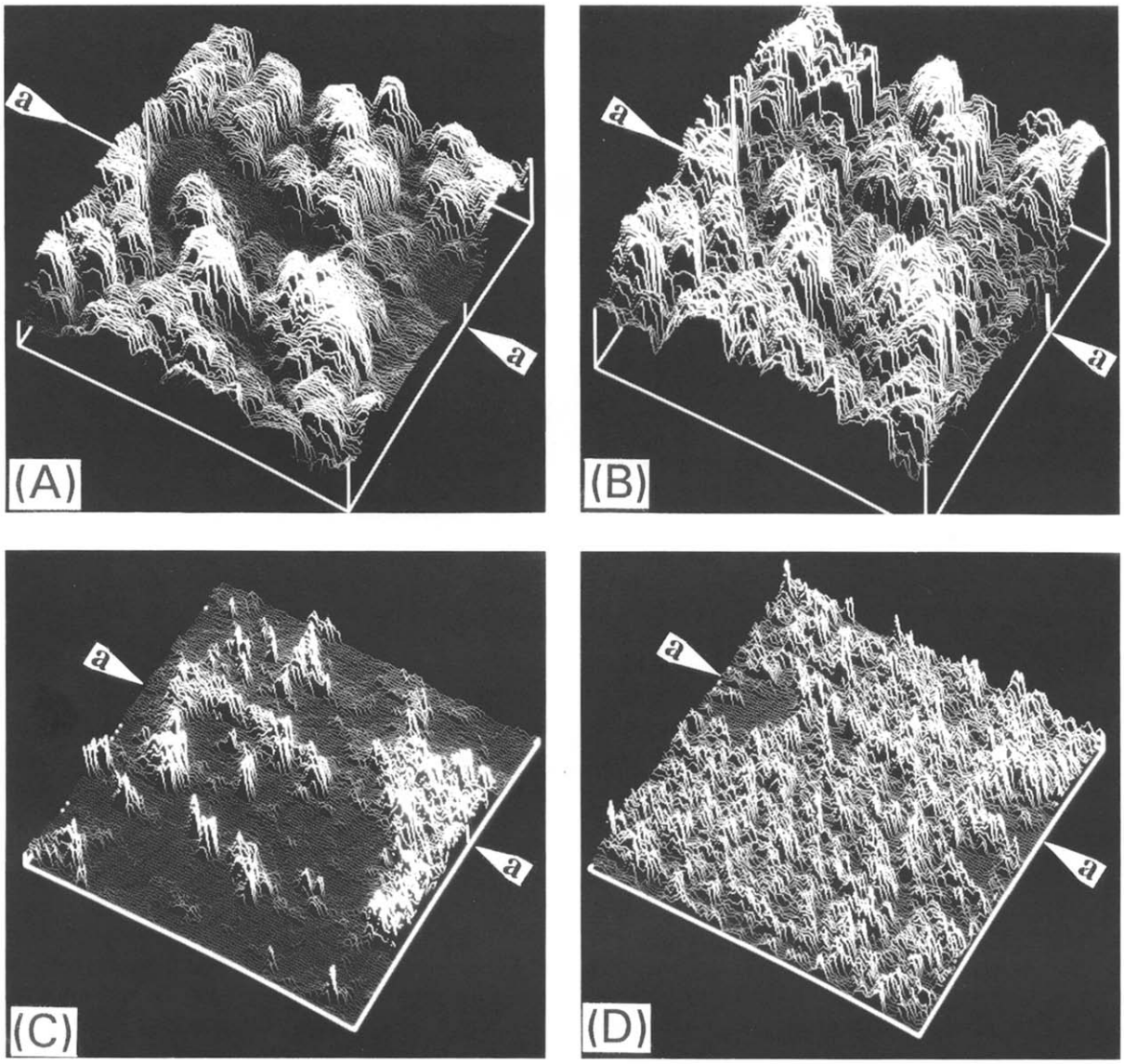

Fig. 5. An area of $1.4 \times 1.4\ \mu m^2$ of a tungsten specimen with TiN deposition in islands investigated by STM using a tungsten tip. (A) is the topographic image of the surface in water, where the top–bottom distance of the recording is 0.11 μm, while (B) is the corresponding surface in air, for which the top–bottom distance is 0.17 μm. (C) and (D) show the tunneling barrier signals recorded simultaneously with (A) and (B), respectively. (E) and (F) show the topography of the cross-section **a–a** in the images (A) and (B), respectively. (G) and (H) show the tunneling barrier signals of the cross-section **a–a** in (C) and (D), respectively.

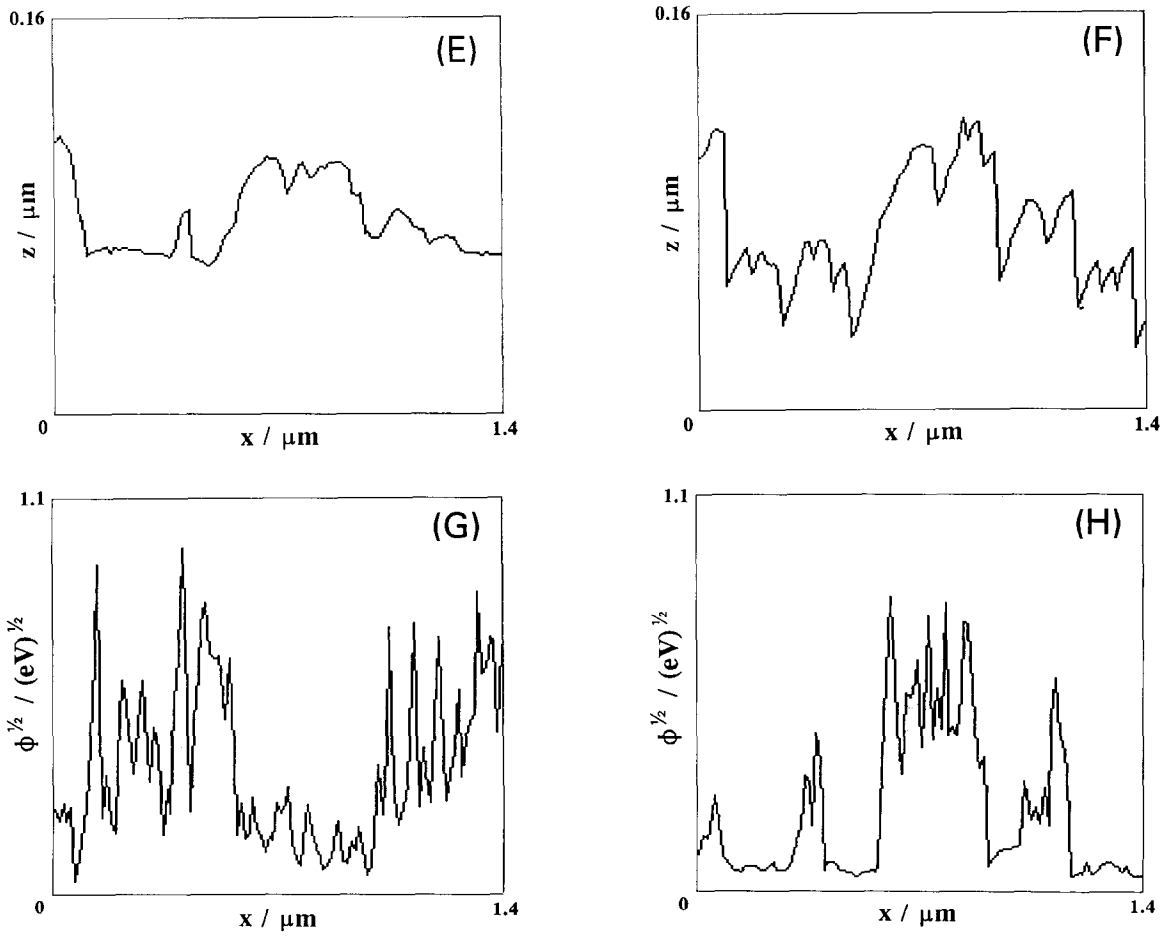

Fig. 5 (continued).

yields two signals: a reference signal due to W–W tunneling and a signal due to tunneling between the coating material and the tungsten tip. Such surfaces were studied on specimens with microcrystals of TiN grown by chemical vapour deposition (CVD) on a tungsten substrate. TiN deposition on the W substrate was carried out for a short time (3 min. for those presented) at a pressure of 200 Pa. In the CVD reactor H_2, N_2, and $TiCl_4$ are used as reactive gases, and TiN grows to form islands on the tungsten substrate, while the tungsten itself does not react with the gases [17]. The outermost surface layer of specimens fully covered by TiN crystals, which is particularly important by STM, was found by Auger electron spectroscopy to be TiO_2.

For STM investigation of (TiN on W)-specimens a sharp tungsten tip was used and the bias voltage on the tip was $V_t \approx -80$ mV (for specimens exposed to TiN deposition for 3 min), the value being determined by the demand for a negligible Faradaic current during operation in water.

The images shown in figs. 5A–5H are representative of these investigations. An area of about 1.4×1.4 μm^2 of a specimen with TiN crystals on W is recorded. As the surface of the TiN deposit (actually TiO_2) could not be drained quickly, the surface exposed to air was recorded before the surface was exposed to water. In figure 5A the topography of the (TiN on W)/water surface is presented, and in fig. 5B the topography of very

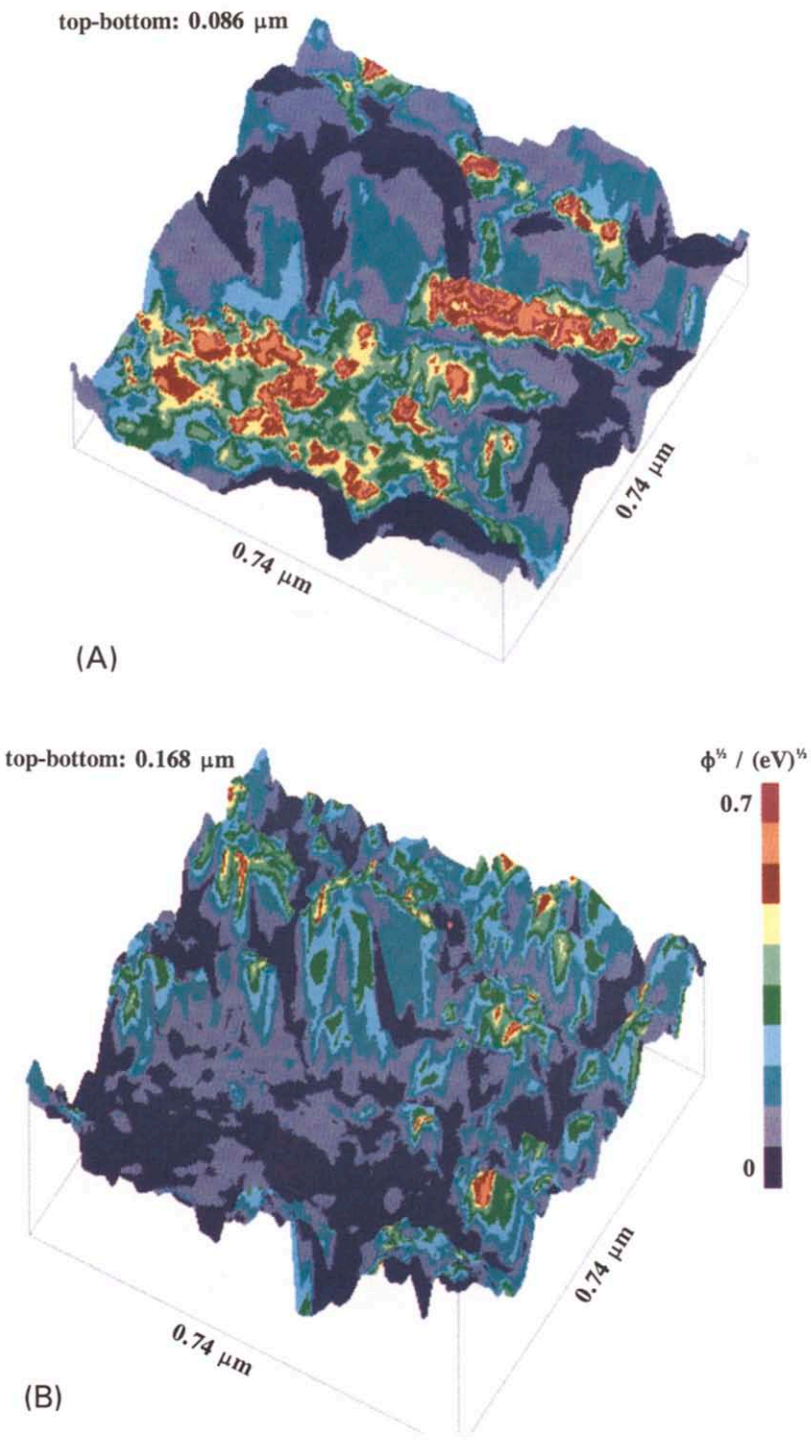

Fig. 6. "Four-dimensional" images of an area of $0.74 \times 0.74\ \mu m^2$ from the same specimen as used for fig. 5. (A) was recorded in water. (B) was recorded in air just before (A). The level of the local tunneling barrier signal is indicated by the colour scale bar.

closely the same area of the (TiN on W)/air surface is shown. The hills are formed by TiN, while the valleys are either W, or W with a thin layer of TiN. It is apparent that the surface exposed to water is more smooth in the microstructure than the one exposed to air. Figs. 5C and 5D show the corresponding tunneling barrier signals, recorded simultaneously with the topographic images. In water the tunneling barrier signals from the hill regions consisting of TiN are low, while in the valleys they are high and irregular. In air the tunneling barrier signals are mostly high and irregular, they are low only in some of the valley areas. These features may be quantified more precisely by considering the cross-section **a–a** in figs. 5A–5D, cut as far as possible in the same place on the wet and the dry surfaces and so that hills as well as valley areas are represented. Figs. 5E and 5F show the topographic cross section **a–a** in the figs. 5A and 5B, respectively. In water, valleys and hills appear to be without significant surface irregularities. In air, the same cross section presents several surface irregularities of width around 100 nm and of depth 10–30 nm. Thus, in water the recorded surface is in most places an envelope of only the large-scale surface structures. Figs. 5G and 5H show the cross-section **a–a** of the tunneling barrier signals in figs. 5C and 5D, respectively. At the TiN hills the tunneling barrier signal changes from values in the range 0.2–0.8 $(eV)^{1/2}$ in air to values in the range of 0.1–0.3 $(eV)^{1/2}$ in water, i.e. a general drop of the tunneling barrier signal. In the valley areas a rise from about 0.1 $(eV)^{1/2}$ in air to the range of 0.3–0.8 $(eV)^{1/2}$ in water occurs. These valley observations are in conformity with the results from fig. 3 and show that even though large structures of TiN have developed, areas with tunneling barrier signals corresponding to naked W still exist.

The above findings, in particular the occurrence of apparently coherent areas of naked tungsten are further illustrated by figs. 6A and B, which show a "four-dimensional" (TiN on W)-surface in water and in air, respectively, of area $0.74 \times 0.74\ \mu m^2$. The specimen is the same as in fig. 5 (but observed at a different location), and also recorded with a sharp tungsten tip. Fig. 6B was recorded before fig. 6A. In the front part of the observed area a valley is located, and here the tunneling barrier signals obtained in water and air reveal spots of uncoated tungsten. The valley is placed between hills of TiN. In air the tunneling barrier signals in the valley is at all locations below 0.2 $(eV)^{1/2}$ (dark and bright violet). They shift to higher levels when water is supplied to the surface. Some valley areas shift to as much as about 0.5–0.7 $(eV)^{1/2}$ as also found in fig. 3 for W–W tunneling and these areas are therefore considered to be uncoated tungsten. Other valley-areas shift to intermediate barrier signal levels, and they may be covered by a thin layer of initial phases of TiN [18]. The corresponding change of the tunneling barrier signal for the hill regions is from values in the range of 0.2–0.5 $(eV)^{1/2}$ (dark blue to brown) in air to values predominantly below 0.2 $(eV)^{1/2}$ (dark blue to light violet) in water, i.e. a decrease of the barrier signal at the supply of water. Fig. 6 is produced by interpolation between neighbouring line scans, while figs. 3 and 4 are made from line scans only. STM investigations of specimens prepared by TiN deposition for different times show that the W areas shrink at increasing deposition time and eventually the tunneling barrier signals interpreted to be connected to W disappear, indicating that after 10 min of deposition in the CVD reactor the specimen is fully covered by TiN [18], which is also confirmed by Auger spectroscopy.

3. Discussion

The experimental results presented above show that by STM it is possible to investigate the same area of a specimen with and without water.

For the interpretation of topographic information from STM images of surfaces exposed to air and water it is important that the STM tip is sharp and that the form of the tip remains the same from one image to the next. Actually, it was found by high resolution electron microscopy (HREM) that the tungsten STM tips are flattened by repeated scannings, in particular by scanning in air on specimens of tungsten and TiN, much less on gold. If the tip is worn the

resolution of the STM decreases during scanning, so that fine surface structures disappear and valleys appear more narrow, hills wider and with a plateau on the top. The tip wear keeps the tungsten tips almost oxide free during scanning. As solid surfaces exposed to water cause significantly less tip wear than when they are exposed to air it is preferable for the comparison of wet and dry surfaces to start investigating the wetted interface and then to drain it, if possible. This is apparent from fig. 3. It is beyond doubt that the wear of the tips is due to contact between tip and specimen when poorly or non-conducting surface elements (e.g. oxides or contamination) locally dominate the tunneling gap during scanning.

In water an orderly structure (ice-Ih) of hydrogen bonded water molecules adjacent to the solid surface is expected to reduce the effective tunneling gap and to allow tunneling also along the solid surface, so that tip–specimen contact is avoided even if locally the specimen surface is non-conducting. Such a structure of water may also explain the character of the tunneling barrier signals observed in water, figs. 2B and 2C. During tip motion toward the solid surface an orderly liquid structure is likely to be crushed or the hydrogen bonds at least bent, so that a relatively high tunneling barrier signal, maybe as in bulk water, is found. During withdrawal of the tip a liquid structure is given space to organize itself, and now tunneling between the closely linked hydrogen-bonded water molecules is supposed to result in a low tunneling barrier. In this case structural reorganization may cause an abrupt shift of the tunneling current or a shift of the tunneling barrier signal. The electric field in the tunneling gap may strain an existing orderly liquid structure of the polar water molecules at the solid surface, and thus weaken the structure or it may enhance the order in an essentially nonstructured liquid [15]. Likewise, by tunneling in air the inhomogeneity of the electric field will cause attraction of gas phase water molecules. Actually, a small decrease of the tunneling barrier signal obtained with a Pt-tip on an Au-sample was observed when the humidity of the air was shifted from very dry to very humid. Also polarization and subsequent attraction of other gas phase molecules may be important for the tunneling barrier of the gap, and as found in ref. [11] very low pressures favour high tunneling barriers.

By Pt–Au tunneling the effect of water is to change the tunneling barrier signal in the opposite direction of that found by W–W tunneling. We assume that the presence of hydrogen bonded water molecules between the tip and specimen causes a reduction of the effective tunneling gap, which is connected to the distance between the water molecules as well as to the distance between the water molecules and the tip molecules/specimen molecules, not to the actual tip–specimen distance directly. At noble metals, where no oxide layers occur the water molecules are bonded by mirror bonds to the tip and specimen. Therefore, water is expected to reduce the tunneling barrier signal compared with that in air. At tungsten the surface is actually tungsten oxide, and on the specimen this oxide layer may be rather thick, while due to wear the tip may have only a very thin oxide layer. It is expected that the tungsten oxide–water interface causes a high tunneling barrier, which in spite of the water molecules in the gap dominates the tunneling barrier, so that by W–W tunneling the barrier signal increases at supply of water.

It might be argued that the smoothness of a non-planar solid surface in water compared with the same surface in air is due to a larger tip–specimen distance in water than in air. However, changes of the tunneling distance larger than 1 nm are not to be expected. As changes of this order are small compared with the radius of the tip apex they are not important for the resolution of the STM. Recordings of surfaces drying up during scanning do not reveal z-level changes of the tip at shift from a wet to a dry surface, which shows that actually the change of tunneling distance is very small [15]. Therefore the recorded smoothness of the surface topography in water can be considered real, and it suggests that further investigation is made of the model of liquid detachment and formation of nano-voids at non-planar solid surfaces exposed to water, as presented in refs. [8,9], a model which apparently can explain a number of well documented [6], but till now apparently inconsistent experimental re-

sults from research in tensile strength of liquids and liquid cavitation.

Acknowledgements

This work was carried out at the Physics Department, DTH and the Danish Institute of Fundamental Metrology with financial support from the Daloon Foundation to J.P. Song during his stay in Denmark as a guest scientist. The Daloon Foundation is gratefully acknowledged. We thank Drs. J. Garnæs, L.L. Madsen and J.F. Jørgensen for helpful discussions. N.H. Pryds and K. Glejbøl are acknowledged for providing us with tungsten samples with TiN deposition and Dr. I. Chorkendorff and Mr. J. Larsen for Auger electron spectroscopy of these samples. Finally the authors wish to thank the referees of Surface Science for valuable suggestions for improvement of the manuscript.

References

[1] R. Sonnenfeld and P.K. Hansma, Science 232 (1986) 211.
[2] J.X. Mou, W.J. Sun, J.J. Yan, W.S. Yang, C. Liu, Z.H. Zhai, Q. Xu and Y.C. Xie, J. Vac. Sci. Technol. B 9 (1991) 1566.
[3] L.L. Madsen, J.F. Jørgensen, K. Carneiro, M. Jørgensen and K. Brunfeldt, Dan. Kemi 6/7 (1992) 28.
[4] M.J. Heben, R.M. Penner, N.S. Lewis, M.M. Dovek and C.F. Quate, Appl. Phys. Lett. 54 (1989) 1421.
[5] L.A. Nagahara, T. Thundat and S.M. Lindsay, Rev. Sci. Instrum. 60 (1989) 3128.
[6] M. Greenspan and C.E. Tschiegg. J. Res. Natl. Bur. Stand., Sect. C, 71 (1967) 229.
[7] W. Drost-Hansen, Chemistry and Physics of Interfaces II (Am. Chem. Soc., Washington, DC, 1971) p. 207.
[8] K.A. Mørch, Proc. Int. Symp. on Modelling Cavitation Phenomena Wuhan, People's Republic of China, 1991, p. 12.
[9] K.A. Mørch, Proc. 2ème Journees Cavitation, Paris, France, Paper 1/18.3, 1992, Soc. Hydrotech. de France.
[10] M.P. Everson and M.A. Tamor, J. Vac. Sci. Technol. B 9 (1991) 1570.
[11] G. Binnig, H. Rohrer, C. Gerber and E. Weibel, Appl. Phys. Lett. 40 (1982) 178.
[12] P.J. Bryant, H.S. Kim, R. Yang, Y.C. Cheng and R. Miller, J. Vac. Sci. Technol. A 6 (1988) 534.
[13] L.L. Madsen, Scanning Tunneling Microscopy, PhD, Thesis, Danish Institute of Fundamental Metrology and Laboratory of Applied Physics, Technical University of Denmark (1990).
[14] J.P. Song, K.A. Mørch, K. Carneiro and A.R. Thölén, Investigation of STM Tunneling Barrier Signals in Air and Water, STM'93 Beijing, People's Republic of China.
[15] K.A. Mørch and J.P. Song, STM for Investigation of Cavitation Nuclei in Liquids, STM'93, Beijing, People's Republic of China.
[16] J.P. Song, N. Hamawi, K. Glejbøl, K.A. Mørch, A. Thölén and L.N. Christensen, Rev. Sci. Instrum. 64 (1993) 900.
[17] N.N. Hamawi and K. Glejbøl, Micron Microsc. Acta 23 (1992) 167.
[18] J.P. Song, N.H. Pryds, K. Gleibøl, K.A. Mørch and K. Carneiro, Studies of TiN Nucleation and Growth by Scanning Tunneling Microscopy in Water, STM'93, Beijing, People's Republic of China.